Supplementary information

Adherens Junctions determine the apical position of the midbody during follicular epithelial cell division

Eurico Morais-de-Sá and Cláudio E. Sunkel

Supplementary Figures and Legends

Figure S1 Apical midbody positioning visualized by different midbody and MR markers

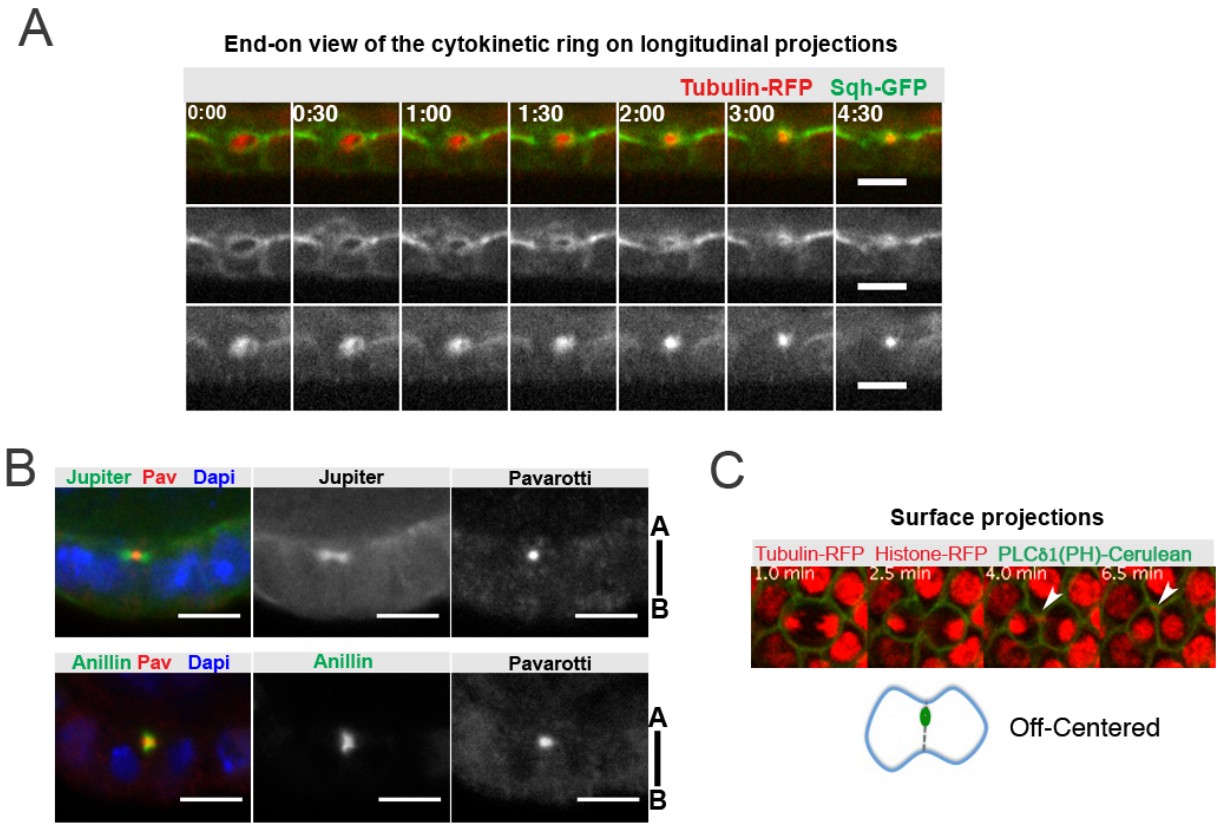

(A) Time-lapse showing an end-on view of the constriction plane and labelled with Sqh-GFP shows the compactation of the midbody associated mictotubules (Tub-RFP) during the CR to MR transition (B) Longitudinal view showing a cross section of the midbody labelled with its associated microtubules show the accumulation of the member of the centraspindlin complex Pavarotti/MKLP1 [1] at the midbody, which is within the midbody ring labelled with Anillin. (C) Frames from a time-lapse of follicle cells expressing Tub-RFP, His-RFP and PLCδ1(PH)-Cerulean as a membrane marker. Projection at the surface of the egg chamber show off centred positioning of the midbody, closer to one neighbour cell. Scale bars = 5 µm.

Figure S2 The Septin Peanut is not required for apical midbody positioning

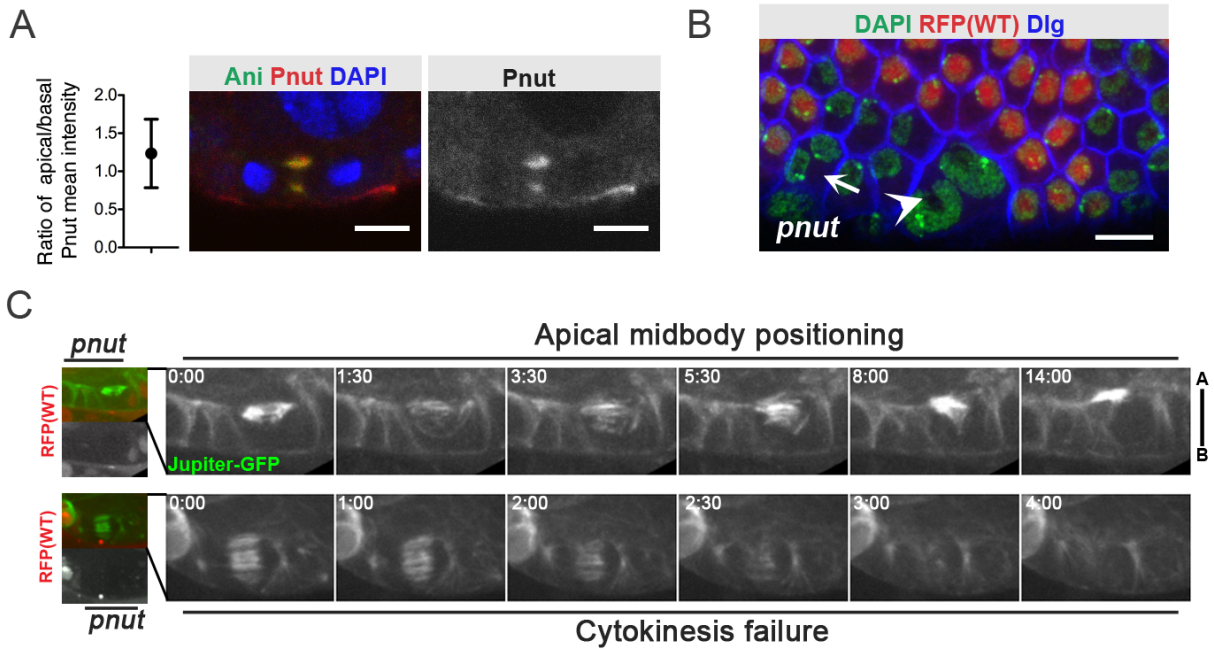

(A) Confocal projections of follicle cells stained with Anillin (green) and Pnut (red) and DAPI (blue). Plot of the apical to basal ratio of Pnut intensity is shown (CR diameter 2-4 µm, average ± SD = 1.23 ± 0.44, n = 11). (B,C) Egg chambers with *pnt*^{KG00478} mutant clones, which are marked by absence of nuclear RFP. (B) *pnt* mutant tissue presents binucleated cells (arrow), some of which with nucleous with abnormal size (arrowhead). Dlg (blue in B) and DAPI (green staining is shown. (C) Live imaging of *pnut* mutants expressing Jupiter-GFP show a mutant cell that fails to compact the midzone microtubules during constriction and fails cytokinesis (bottom). Midbody microtubules are always positioned apically whenever *pnut* cells reach the stage of midbody formation (Top, 100 %, n = 15). Scale bars = 5 µm.

Figure S3: *rok* follicle cells maintain AB polarity and complete cytokinesis with a lower constriction rate

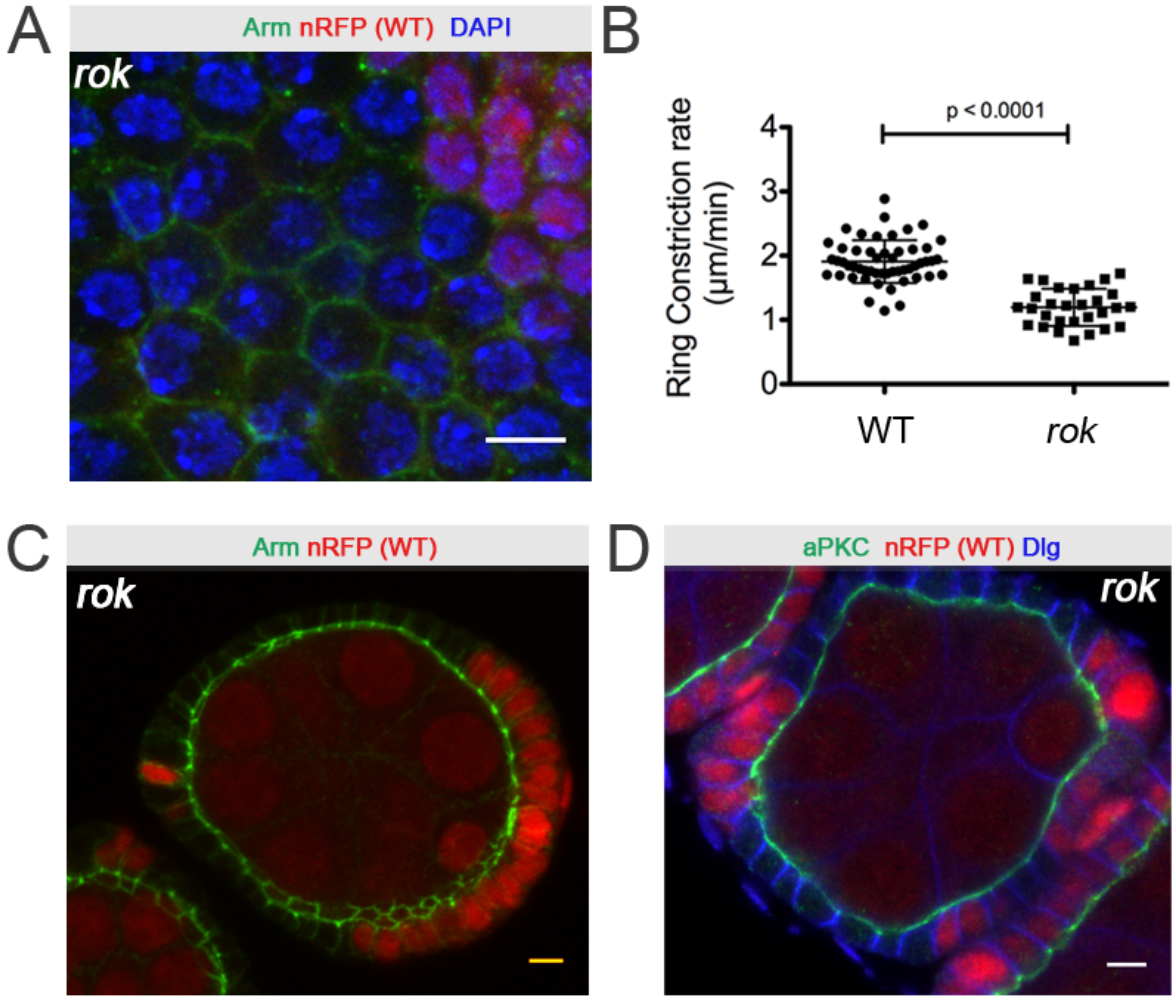

(A,C,D) Egg chambers with *rok*^{2} mutant clones, which are marked by absence of nuclear RFP, and stained for Arm (green in C), DAPI (Blue in A) and aPKC (green in D) and Dlg (blue in D). (A) Large *rok* mutant clones show only cells with single nucleus and (C,D) display wild-type localization of the AJ marker Arm, as well as apical localization of aPKC and lateral localization of Dlg (C). (B) Quantification of the constriction rate for WT (1.91 ± 0.33 µm/min, n=52) and *rok*^{2} (1,19 ± 0.29 µm/min, n=29) mutant cells (see supplementary methods for details).

Figure S4: Mitotic depolarization of the apical Par-6/aPKC polarity proteins

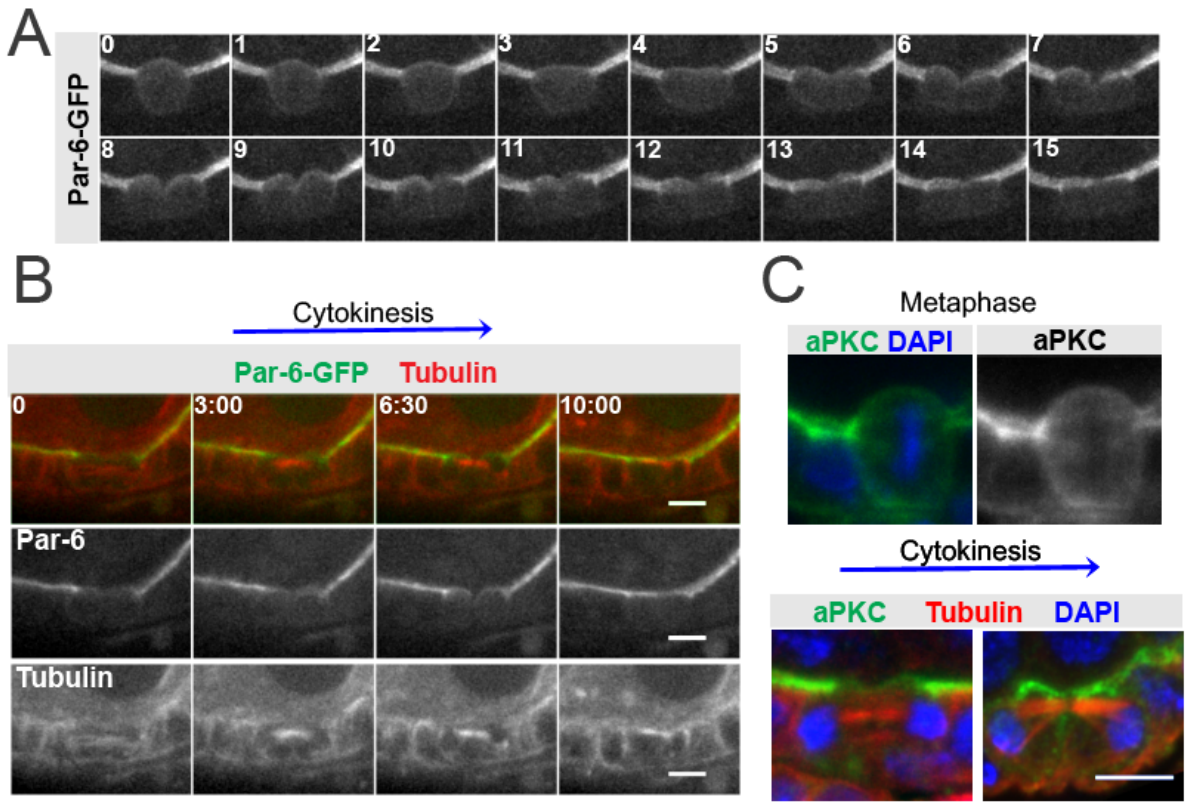

(A,B) Longitudinal time-lapse projections of follicle cells expressing Par-6-GFP and Tubulin-RFP (B) show depolarization of Par-6-GFP division (A) and that the apical distribution of Par-6 is not yet established at the beginning of cytokinesis, but is established upon apical midbody positioning (B). (C) Follicle cells stained for DAPI (blue), aPKC (green) and α-tubulin (red, below).

Figure S5: Asymmetric midbody positioning within the apical surface of the epithelium correlates with the organization of AJ

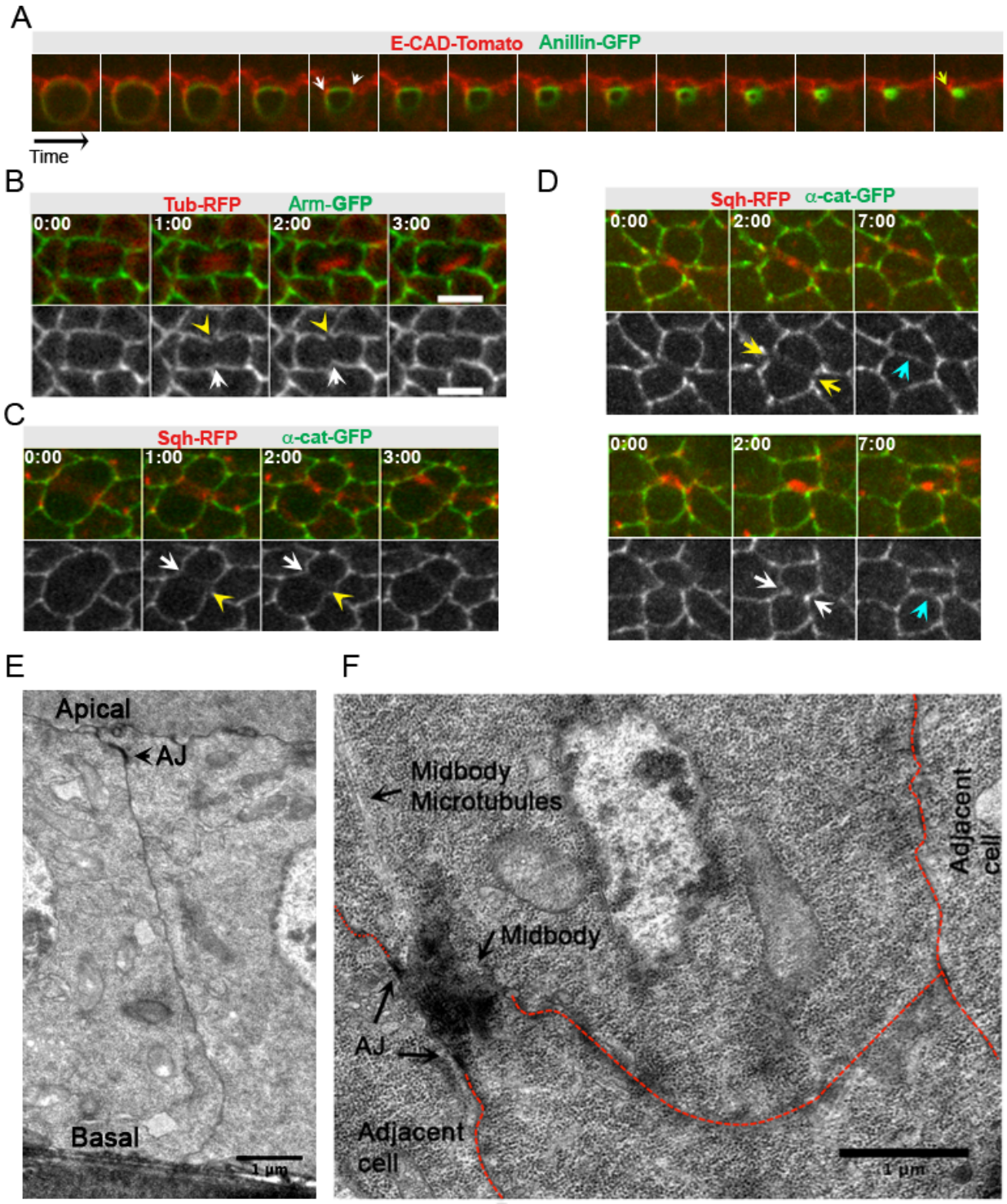

(A) Sequential frames from a longitudinal time-lapse showing an end-on view of the CR (Anillin-GFP) to allow the visualization of the AJs formed with both neighbour cells within the same plane. Note that AJs on both sides, marked with E-Cad-Tomato, maintain the connection to the CR during the initial phases of constriction (white arrows), but the midbody later remains coupled to AJ at only one adjacent side (yellow arrow). (B) Frames from time-lapse movies showing a surface view of follicle cells expressing Tub-RFP and Arm-GFP or (C,D) Sqh-RFP and α-Cat-GFP (B,C) Apical Midbody positioning shows asymmetry within the apical surface (74.3%, n=70), being closely associated to AJs formed with one neighbouring cell (white arrows). Markers of AJ present reduced levels in the region that is uncoupled from the CR (yellow arrow). (D) Less frequently, we observed that the midbody displays a centred position along the apical surface, remaining connected (11.4%, white arrows) or disengaging (14.3%, yellow arrows) simultaneously from both sides. Scale bar = 5 μm
(E) TEM picture showing a section parallel to the AB axis, where the electron-dense AJ is observed close to the apical surface. (F) TEM micrograph showing a section nearly parallel to the apical surface reveals the close proximity between AJs formed with one neighbouring cell and the midbody, visualized as electron-dense material and its associated microtubules. The membranes between the daughter cells and their neighbours are marked in red (E,F) Scale bar = 1 μm.

Figure S6: Expression of *DE-CAD-α-cat-GFP* rescues epithelial organization and midbody positioning in *arm* mutant cells.

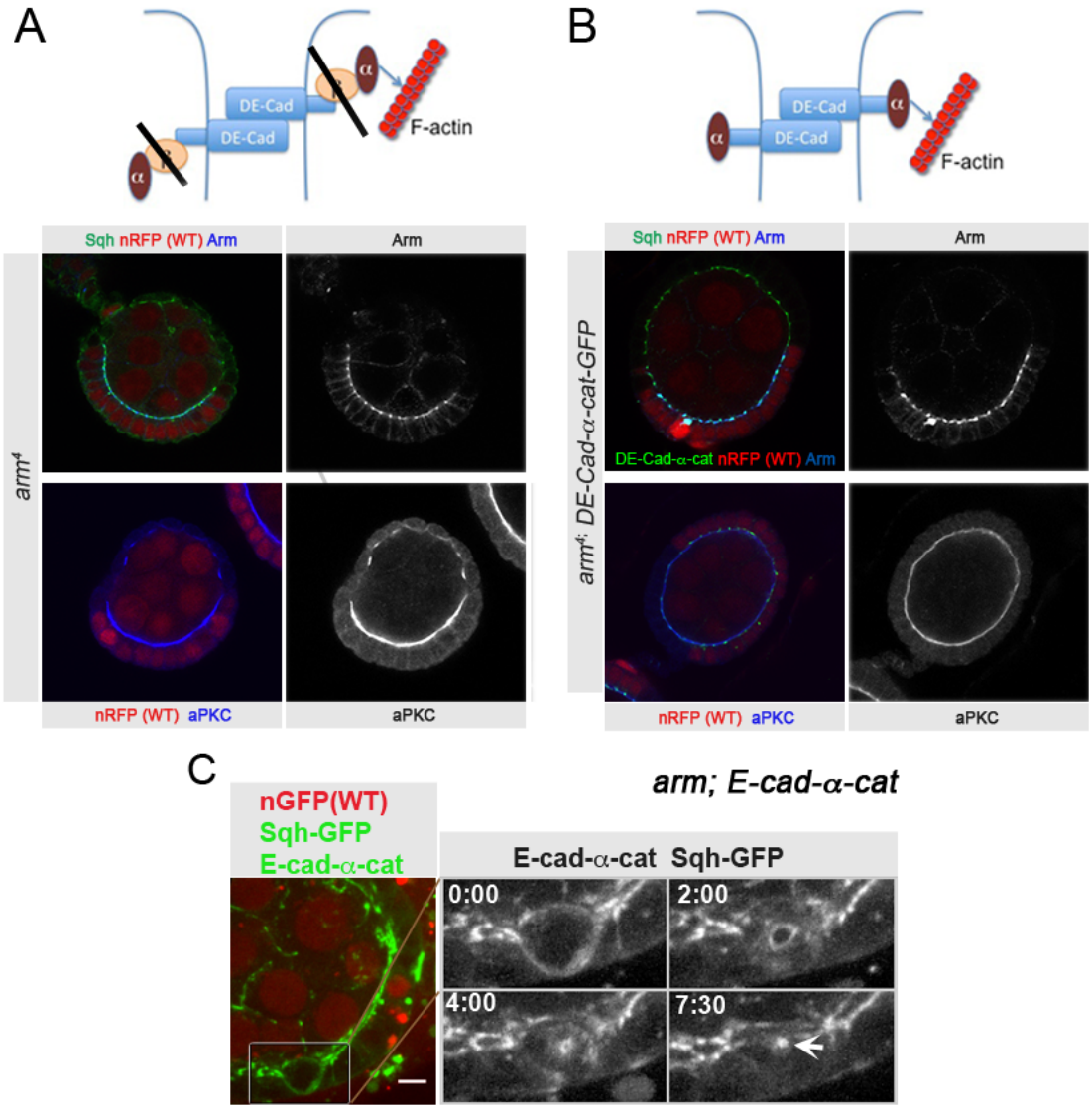

(A,B) *arm*^{4}; Sqh-GFP (A) and *arm*^{4} ; DE-CAD-α-cat-GFP (B) clones are marked by absence of RFP, and stained for Arm and aPKC. Note the rescue of epithelial integrity and polarity by expression of DE-CAD-α-cat-GFP, despite absence of any Arm staining in *arm* mutant clones. (C) A large *arm*^{4} clone expressing DE-CAD-α-cat-GFP and Sqh-GFP displays apical midbody positioning.

Figure S7: Midbody mispositioning in *dlg* mutant cells

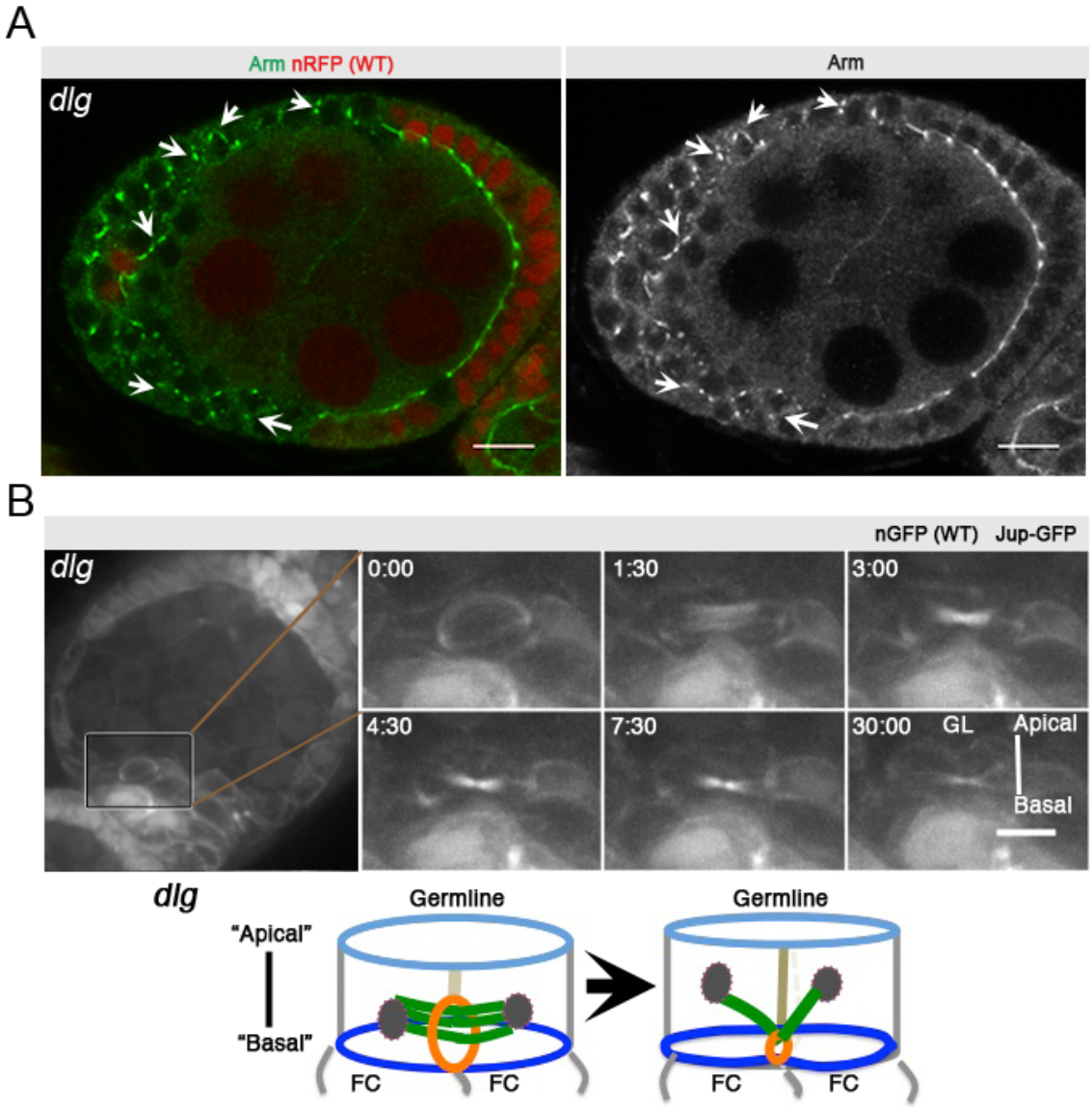

(A) Egg chambers with dlg^{IP20} mutant clones marked by absence of nuclear RFP (red) and stained for Arm (green). *dlg* mutants form multiple layers of follicle epithelial cells and misplace AJs (arrows) that can be formed with more basal follicle cells. (B) Live imaging of *dlg* mutants (marked by absence of nuclear GFP) expressing Jupiter-GFP show ectopic positioning (65.2 %, n = 23) of the midbody microtubules along the AB axis (white arrow). It should be noted that only dividing cells that have direct contact with the germline were used for quantification, so that "apical" could be defined as the side contacting the germline and "basal" the opposite side. Scale bar = 5 µm. The diagram at the bottom illustrates how misplaced AJs (dark blue), which are formed with follicle cells (FC) present below due to multilayering, may result on midbody misplacement. The contractile ring (orange), microtubules (green) and the putative apical side, where AJ are present in the wild type (light blue) are shown. See also movie S7.

Figure S8 – F-actin polymerization at the daughter cell interface is spatially oriented by the midbody

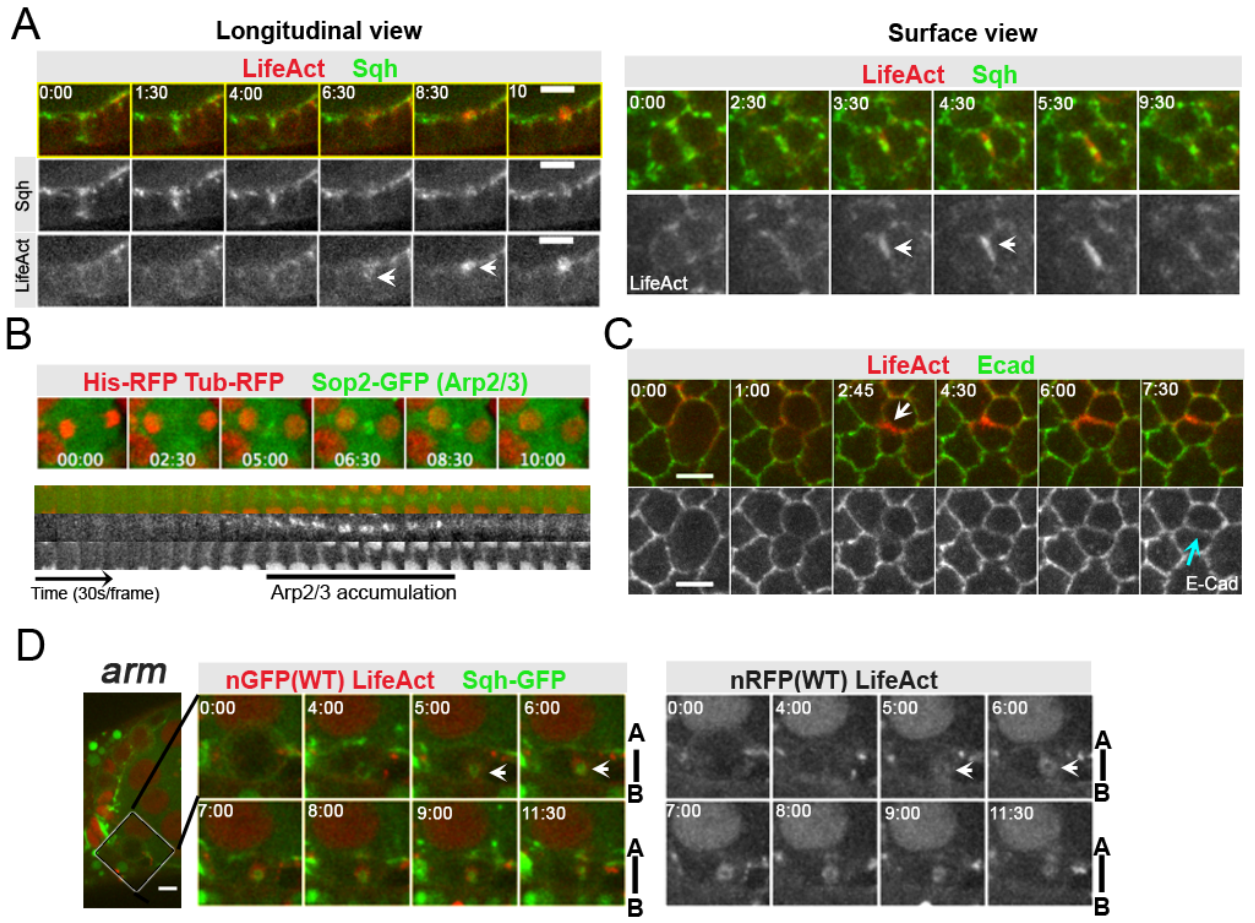

(A) Frames from time lapse projections with longitudinal and surface views of follicle cells expressing Sqh-GFP and LifeAct-Ruby. Fast actin polymerization starts upon cytokinetic constriction around the midbody (white arrows). (B) Frames from time lapse projections showing surface views of cells expressing SOP2-GFP, His-RFP and Tub-RFP. Kymograph is shown below. SOP2, which encodes for one subunits of the ARP2/3 complex (Arpc1), transiently accumulates close to the midbody (marked by compact microtubules). (C) Frames from time lapse surface movies of cells expressing DE-Cad-GFP and LifeAct-Ruby. Actin polymerization (white arrow) preceeds the formations of stable adherens junctions at the interface between daughter cells (cyan arrow). (D) Time-lapse projection of longitudinal sections in *arm*^{4} mosaic egg chambers. Mutant cells are marked by absence of nuclear RFP, and are expressing Sqh-GFP and LifeAct-Ruby. Frames from longitudinal time-lapse projections show that despite midbody mispositioning, actin polymerization occurs around the midbody in *arm* mutants (arrows). Red channel is also shown as separate panel.

Supplementary Movies

Movie S1, Asymmetric cleavage furrow ingression in *Drosophila* follicle cells

Time-lapse movies of follicle cells expressing Sqh-GFP and Myr-Tomato (top); Sep2-GFP (middle); Anillin-GFP and His-RFP (Bottom). This is an assembly of four movies showing that furrow ingression starts from the basal side (top) and also that Sqh, Septin2 and Anillin localization is nearly symmetric along the AB axis of the contractile ring. Note that the movie shows examples of cells whose plane of constriction is parallel (right, dividing along Z, and therefore showing end-on views of the ring) or almost perpendicular (left, dividing along X, showing cross-sections of the ring) to the plane of imaging.

Movie S2, Follicle cell division in *rok* mutants

Time-lapse movies of a mosaic egg chambers containing rok^2 clones (labeled by RFP absence) and expressing Sqh-GFP. The CR can display basal directed constriction in rok^2 cells (11:00), but the CR is quickly positioned at the apical domain (15:00). A wild-type cell dividing in a different focal plane within the same egg chamber is shown on the right.

Movie S3 The contractile ring is closely associated to Adherens Junctions during cytokinesis

Longitudinal time-lapse projection of follicle cells expressing Sqh-GFP and DE-CAD-Tomato (Top), Ani-GFP and DE-CAD-Tomato (Bottom). AJs are closely connected to the apical side of the contractile ring during constriction.

Movie S4, Asymmetric coupling of the Midbody to one neighboring cell AJ.

Time-lapse movies of follicle cells expressing Sqh-GFP and DE-CAD-Tomato (top), αCat-GFP and Sqh-RFP (Bottom), show follicle cells where the CR is asymmetrically coupled to AJs formed with adjacent cells at one side, leading to an asymmetry of midbody positioning within the apical side.

Movie S5, Follicle cell division in *arm* mutants

Time-lapse movie of a mosaic egg chambers containing arm^4 clones (labeled by RFP absence) and expressing Sqh-GFP. This movie shows two arm^4 cells where apical directed constriction of the ring is disrupted and the midbody fails to be positioned on the apical side of the cell. A close up of the green channel in the boxed region is shown below.

Movie S6, Follicle cell division in *dlg* mutants

Time-lapse sequences showing a mosaic egg chamber containing *dlg* clones (labeled by nuclear GFP absence and contoured) expressing Jup-GFP and His-RFP. Mutant cells display basal positioning of the midbody associated microtubules (arrow).

Movie S7, Midbody is directed to wild-type neighbours when wild-type cells divide alongside *arm* mutant cells
Time-lapse sequence of surface projections of mosaic egg chambers containing arm^4 clones (labeled by RFP absence). Wild-type cells direct the midbody (labeled by its associated microtubules (Jup-GFP)) away from the *arm* clone, in direction to the wild-type cell.

Movie S8, Recruitment of the midbody by Ed-GFP-Ecadi adhesion sites in S2 cells
Time-lapse movies of a S2 cells expressing Cherry-Tubulin and Ed-GFP (left movie) or Ed-GFP-Ecad(i) (right movie). Tubulin is shown below as a separate channel. The midbody microtubules are efficiently recruited to the cell-cell contact site when ED-GFP-ECadi is expressed.

Movie S9, The Arp2/3 complex displays a transient accumulation around the midbody
Time-lapse movie of projections at the surface of an egg chamber expressing Sop2-GFP (green) to mark the localization of the Arp2/3 complex, His-RFP(red) and Tub-RFP(red). Midbody is visualized by associated compact microtubules.

Movie S10, Ectopic midbody positioning disrupts epithelial architecture
Time-lapse movie of follicle cells expressing LifeAct to follow actin dynamics, and Par-6 GFP to mark the apical domain. Cells expressing Dg-ECADi are shown at the bottom.

Supplementary Methods

Drosophila strains and genetics

w^{1118} was used a wild-type strain. The following mutant alleles and transgenic lines that were used are described in Flybase (www.flybase.org) and were either obtained from BDSC, DGRC or the fly community: rok^{2} [15]; dlg^{ip20}[2]; arm^{4} [3] (Gift of P.Rorth); $pnut^{KG00478}$*; DE-Cad-Tomato, DE-CAD-αCat-GFP* and *DE-CAD-GFP* [4] (Gift of Y.Hong); *αCat-GFP*^{CPTI002516}, arm-GFP^{CPTI001198}*; Sqh-GFP* [5] (Gift of R.Karess) and Sqh-RFP [6]; *His2av-mRFP* [7]; *Par-6-GFP* [8](Gift of J.Knoblich); *Sep2-GFP* and UAS::Anillin-GFP (Gift of A.Wilde) [9]; *UASp::GFP-Rho1* (BL#9392); *UAS::myr-tdTomato* [10]*; UAS::Sop2-GFP* [11]; UAS::PLCδ1(PH)-Cerulean (BL#31421); UAS:LifeAct-GFP (BL#35545); *UAS::Dg-ECADi-Δβ* and *UAS::Dg-ECADi* (this study) and UAS:LifeAct-Ruby (BL#35545) were used to follow actin dynamics, since LifeAct is small peptide that binds F-actin without affecting actin dynamics [12]. Stocks with endogenous expression of the microtubule binding protein Jup-GFP [13] were used to label microtubules [14]. We used GR1::GAL4 [15] (Gift of T.Schupbach) to induce expression of UAS transgenes in the follicle epithelium as it drives expression since early oogenesis, allowing the analyses of mitotic stages. In order to achieve higher expression levels during early oogenesis, flies with transgenes driven by GR1::GAL were cultured at 29ºC during at least one day prior to dissection. Clonal analyses were performed using the FLP/FRT-mediated mitotic recombination system [16].
Standard *Drosophila* methods were used to generate the different genotypes, which are shown below.

Figure 1

B.D.	*w; ; Jup-GFP His2av-mRFP*
E	*w*; *Sqh-GFP*/*UAS:: myr-tdTomato*; *GR1::GAL4*/ +
F	*w*; *His2A-RFP Tub-RFP*/+ ; *GR1::GAL4*/ UAS::PLCδ1(PH)-Cerulean
G	*w; Sqh-GFP*

Figure 2

A^{Top}	*w*; *His2A-RFP Tub-RFP*/+; *UAS::Ani-GFP/GR1::GAL4*
A^{middle}	*w*; *His2A-RFP Tub-RFP*/+; *Sep2-GFP*/+
A^{Top}	*w UASp::GFP-Rho1*; *His2A-RFP Tub-RFP*/+; *GR1::GAL4*/+
B	*w*
C	*y w* rok^{2} *FRT19A/y w ubi::nls-GFP FRT19A ; e22c::GAL4 UAS::FLP /+*
D,E	y *w* rok^{2} *FRT19A/ w ubi::nls-RFP hs::FLP ; Sqh-GFP / +*

Figure 3

A,B	*w*; *DE-Cad-Tomato*/Sqh-GFP
C	*w*
D.E.F^{Top}	arm^{4} *FRT19A/w ubi::nls-RFP hs::FLP; Sqh-GFP/+*
E	arm^{4} *FRT19A/w ubi::nls-RFP hs::FLP; Sqh-GFP/DE-CAD-αCat-GFP*
F^{Bottom}	arm^{4} *FRT19A/w ubi::nls-RFP hs::FLP; Jup-GFP/+*

Figure 4

A	w ;; *GR1::GAL4/ UAS::Dg-ECADi-Δβ*
A	w ;; *GR1::GAL4/ UAS::Dg-ECADi*
C^{top}	w ;; *UAS::LifeAct-GFP/+*; *GR1::GAL4/+*
C^{middle}	w ;; *UAS::LifeAct-GFP/+*; *GR1::GAL4/ UAS::Dg-ECADi*
C^{bottom}	*par6::Par-6-GFP/+*; *UAS::LifeAct-Ruby/+*; *GR1::GAL4/ UAS::Dg-ECADi*

Figure S1

A	*w; Sqh-RFP/+; Jup-GFP*
B^{top}	w ;; *Jup-GFP*
B^{bottom}	w; *GR1::GAL4/ UAS::Anillin-GFP*
C	*w*; *His2A-RFP Tub-RFP*/+ ; *GR1::GAL4*/ UAS::PLCδ1(PH)-Cerulean

Figure S2

A	*w*
B	*hs::FLP /+; FRT42D pnt*^{KG0047}/FRT42D *ubi::nls-RFP*
C	*hs::FLP /+; FRT42D pnt*^{KG0047}/FRT42D *ubi::nls-RFP; Jup-GFP/+*

Figure S3

A.C.D	y *w rok*^{2} *FRT19A/ w ubi::nls-RFP hs::FLP*
B	y *w rok*^{2} *FRT19A/ w ubi::nls-RFP hs::FLP ; Sqh-GFP / +*

Figure S4

A.B	*par6::Par-6-GFP ; His2A-RFP Tub-RFP/+*
C	*w*

Figure S5

A	*w; DE-Cad-Tomato/+; UAS::Ani-GFP/GR1::GAL4*
B	*Arm-GFP/+; Tub-RFP/+*
C.D	*αCat-GFP/+; Sqh-RFP/+*
E.F	*w*

Figure S6

A	*arm*^{4} *FRT19A/w ubi::nls-RFP hs::FLP; Sqh-GFP/+*
B.C	*arm*^{4} *FRT19A/w ubi::nls-RFP hs::FLP; Sqh-GFP/DE-CAD-αCat-GFP*

Figure S7

A	y *w dlg*^{ip20} FRT19A/ *w ubi::nls-RFP hs::FLP*
B	y *w dlg*^{ip20} FRT19A/*w ubi::nls-GFP FRT19A ; e22c::GAl4 UAS::FLP/+ ; Jup-GFP His-RFP/+*

Figure S8

A	w; Sqh-GFP/UAS::LifeAct-Ruby; GR1::GAL4/+
B	w/ w UASp::Sop2-GFP; His2A-RFP Tub-RFP/+; GR1::GAL4/+
C	w; DE-Cad-GFP/UAS::LifeAct-Ruby; GR1::GAL4/+
D	*arm*^{4} *FRT19A/w ubi::nls-RFP hs::FLP; Sqh-GFP* UAS::LifeAct-Ruby/+; GR1::GAL4/+

Generation of *pUASp-Dg-ECADi* and *pUASp-Dg-ECADi-Δβ lines*

Dystroglycan coding sequence for the extracellular and transmembranar domain was amplified by PCR from *dg* cDNA (clone GH09323, *Drosophila* GOLD cDNA collection) and cloned into the KpnI/BglII sites of pUASp-PL vector [17]. The full intracellular domain of D-Ecad, or lacking 83 aa at the C-term (deletion of the β-catenin binding site [18]), was then cloned into the BglII/XbaI sites of pUASp-Dg, generating t*pUASp-Dg-ECADi* and *pUASp-Dg-ECADi-Δβ*. Since the BglII site encodes for an RS amino acid sequence, which is present in the beginning of the Dg cytoplasmic domain, this strategy generated a fusion that replaces the last 99 aa of the C-term cytoplasmic domain of Dg with the D-Ecad C-term cytoplasmic domain. Transgenesis was performed by standard germline transformation (BestGene Inc).

S2 cell culture and immunofluorescence

Schneider (S2) cells were cultured in Schneider's growth media supplemented with 10% heat-inactivated fetal bovine serum. Stable transfection of recombinant plasmids into S2 cells was performed using Cellfectin® II reagent, Life technology (Invitrogen), according to the manufactures´s instructions. For immunofluorescence analysis of S2 cells, 10^5 cells were centrifuged onto slides for 5min, at 1000 rpm (Cytospin 2, Shandon). Cells were fixed in 4% paraformaldehyde in PBS, followed by three 5 minutes washing steps in PBS-T (PBS with 0.05% Tween 20), 30 minutes incubation in blocking buffer (PBS-T complemented with 10%FBS), and primary antibody incubation overnight.

Primary antibody and dilutions used for immunofluorescence

Rabbit anti-PKCz (1/500, C-20 Santa Cruz Biotechnology), mouse anti-Dlg (1/200, Developmental Studies Data Bank (DSHB)) guinea-pig anti-Baz (1/500, [19], gift of J.Zallen), rabbit anti-Pav (1/750, [1] gift of D.Glover) mouse anti-Arm (1/100, DSHB), mouse anti-α-tubulin (1/1000, B512 Sigma), mouse anti-αCatenin (1/50, DCAT-1 DSHB), mouse anti PNUT (1/100, DSHB), rabbit anti-Anillin (1/500, [20], Gift of J.Brill) and rabbit anti-phospho-MRLC (Ser19) (1:50, Cell Signaling; Ser21 in *Drosophila* Sqh is equivalent to Ser19 in human MRLC [21]). Actin was visualized with FITC/TRITC conjugated phalloidin (Sigma).

Image collection

Images of fixed samples were collected using Leica TCS SP5 II (Leica Microsystems) confocal microscope with a HC PL APO CS 40x/NA 1.10 or a HC PL APO CS 63X/NA 1.3 lens and LAS 2.6 software. Live analyses of cell division were performed on intact *Drosophila* egg chambers dissected into Halocarbon oil 700 (Sigma) as previously described in [22] or for imaging of longer periods in Schneider's *Drosophila* medium supplemented as described in [23]. 4D datasets were collected at 25ºC with a spinning disc confocal system (Andor Revolution XD) equipped with an electron multiplying charge-coupled device camera (iXonEM+; Andor) and a CSU-22 unit (Yokogawa) based on an inverted microscope(IX81; Olympus) with aPLAPON 60x/NA 1.42 or UPLSAPO 100x/1.40 lens, using iQ software(Andor). Z-stacks consisted in a series of 8-10 optical sections to include the planes related to the dividing cell separated by 0.5-1 mm along z-axis. Images shown are maximum projections of all the z-series, which cover the region of interest of the dividing cell.

Data analysis

To quantify fluorescence intensity along the AB axis during cytokinesis (Fig 2A), mean pixel intensity was measured in a boxed area at the cell equator in maximum intensity projections that included the basal and apical sides of the contractile ring. The ratio of Apical/Basal p-Myosin/Pnut intensity (Fig 2B and S2A) was determined by manually delimiting regions with identical area and within the maximum intensity of the Apical and Basal arcs of the contractile ring. The ratio between the mean intensities of the selected areas was then measured after subtracting background intensity. To quantify constriction rate (Fig S3B), the diameter of the ring along the AB axis (d) was measured for consecutive time points (t) in a constriction window corresponding to constant constriction rate. We computed the constriction rate (β - μm/min) as the slope of a linear regression ($d = \alpha+\beta t$; $R^2>0.95$ was set as a threshold for the linear fit to assume constant constriction rate) computed with Prism (GraphPad Software). Normalized

contractile ring position along the AB axis (Fig 2E and Fig3E) was measured as the distance from the basal cortex to the center of the contractile ring normalized to the length of the AB axis of the epithelial monolayer. Image analyses and quantifications were performed with ImajeJ/Fiji, whereas the statistical analysis and graphs were performed with Graphpad software.

Transmission Electron Microscopy

Ovaries were fixed 16h in 1% glutaraldehyde, 1% tannic acid 0.1m cacodylate buffer, pH 7.2 at 4° C. After three 15 minutes washes in cacodylate buffer, ovaries were post-fixed in 2% osmium tetroxide for 1 hour. Following staining with 2% uranyl acetate and dehydration in an acetone series, ovaries were infiltrated and polymerized in Embed 812 resin (Electron Microscopy Sciences) overnight at 60° C. Ultrathin sections (40-60 nm thickness) were prepared on a RMC powerTome XL Ultramicrotome. The sections were mounted on 200 mesh nickel grids, stained with uranyl acetate and lead citrate, and examined under a JEOL JEM 1400 TEM (Tokyo, Japan). Images were digitally recorded using a Gatan SC 1000 ORIUS CCD camera (Warrendale, PA, USA).

Supplemental References

1. Adams RR, Tavares AA, Salzberg A, Bellen HJ, Glover DM (1998) pavarotti encodes a kinesin-like protein required to organize the central spindle and contractile ring for cytokinesis. *Genes & development* **12:** 1483-1494
2. Woods DF, Bryant PJ (1991) The discs-large tumor suppressor gene of Drosophila encodes a guanylate kinase homolog localized at septate junctions. *Cell* **66:** 451-464
3. Peifer M, Rauskolb C, Williams M, Riggleman B, Wieschaus E (1991) The segment polarity gene armadillo interacts with the wingless signaling pathway in both embryonic and adult pattern formation. *Development* **111:** 1029-1043
4. Huang J, Zhou W, Dong W, Watson AM, Hong Y (2009) From the Cover: Directed, efficient, and versatile modifications of the Drosophila genome by genomic engineering. *Proceedings of the National Academy of Sciences of the United States of America* **106:** 8284-8289
5. Royou A, Sullivan W, Karess R (2002) Cortical recruitment of nonmuscle myosin II in early syncytial Drosophila embryos: its role in nuclear axial expansion and its regulation by Cdc2 activity. *The Journal of cell biology* **158:** 127-137
6. Martin AC, Kaschube M, Wieschaus EF (2009) Pulsed contractions of an actin-myosin network drive apical constriction. *Nature* **457:** 495-499
7. Pandey R, Heidmann S, Lehner CF (2005) Epithelial re-organization and dynamics of progression through mitosis in Drosophila separase complex mutants. *Journal of cell science* **118:** 733-742
8. Wirtz-Peitz F, Nishimura T, Knoblich JA (2008) Linking cell cycle to asymmetric division: Aurora-A phosphorylates the Par complex to regulate Numb localization. *Cell* **135:** 161-173
9. Silverman-Gavrila RV, Hales KG, Wilde A (2008) Anillin-mediated targeting of peanut to pseudocleavage furrows is regulated by the GTPase Ran. *Molecular biology of the cell* **19:** 3735-3744

10. Pfeiffer BD, Ngo TT, Hibbard KL, Murphy C, Jenett A, Truman JW, Rubin GM (2010) Refinement of tools for targeted gene expression in Drosophila. *Genetics* **186:** 735-755
11. Hudson AM, Cooley L (2002) A subset of dynamic actin rearrangements in Drosophila requires the Arp2/3 complex. *The Journal of cell biology* **156:** 677-687
12. Riedl J *et al* (2008) Lifeact: a versatile marker to visualize F-actin. *Nature methods* **5:** 605-607
13. Buszczak M *et al* (2007) The carnegie protein trap library: a versatile tool for Drosophila developmental studies. *Genetics* **175:** 1505-1531
14. Karpova N, Bobinnec Y, Fouix S, Huitorel P, Debec A (2006) Jupiter, a new Drosophila protein associated with microtubules. *Cell motility and the cytoskeleton* **63:** 301-312
15. Gupta T, Schupbach T (2003) Cct1, a phosphatidylcholine biosynthesis enzyme, is required for Drosophila oogenesis and ovarian morphogenesis. *Development* **130:** 6075-6087
16. Xu T, Rubin GM (1993) Analysis of genetic mosaics in developing and adult Drosophila tissues. *Development* **117:** 1223-1237
17. Rorth P (1998) Gal4 in the Drosophila female germline. *Mechanisms of development* **78:** 113-118
18. Pacquelet A, Lin L, Rorth P (2003) Binding site for p120/delta-catenin is not required for Drosophila E-cadherin function in vivo. *The Journal of cell biology* **160:** 313-319
19. Simoes Sde M, Blankenship JT, Weitz O, Farrell DL, Tamada M, Fernandez-Gonzalez R, Zallen JA (2010) Rho-kinase directs Bazooka/Par-3 planar polarity during Drosophila axis elongation. *Developmental cell* **19:** 377-388
20. Goldbach P, Wong R, Beise N, Sarpal R, Trimble WS, Brill JA (2010) Stabilization of the actomyosin ring enables spermatocyte cytokinesis in Drosophila. *Molecular biology of the cell* **21:** 1482-1493
21. Jordan P, Karess R (1997) Myosin light chain-activating phosphorylation sites are required for oogenesis in Drosophila. *The Journal of cell biology* **139:** 1805-1819
22. Weil TT, Parton RM, Davis I (2012) Preparing individual Drosophila egg chambers for live imaging. *Journal of visualized experiments : JoVE*
23. Prasad M, Jang AC, Starz-Gaiano M, Melani M, Montell DJ (2007) A protocol for culturing Drosophila melanogaster stage 9 egg chambers for live imaging. *Nature protocols* **2:** 2467-2473